Electrodeoxidation of Iron Oxide in Aqueous NaOH Electrolyte

G. M. Haarberg[a] and B. Khalaghi[a]

[a] Department of Materials Science and Engineering, Norwegian University of Science and Technology (NTNU), 7491 Trondheim, Norway

The production of iron and steel contributes to ~10 % of global CO_2 emissions. Electrolysis is an alternative route to eliminate CO_2 formation. Experiments were carried out in NaOH-H_2O (50-50 wt%) electrolyte with a suspension of Fe_2O_3 particles at ~100 °C. A rotating disk electrode was used as the cathode. Different cathode substrates of different graphite qualities and silver were used. The current efficiency for iron deposition was consistently higher than 90 %. Silver was found to be an excellent substrate for good quality deposits. Cathodes in the form of pellets of hematite were also found to be reduced to iron by electrodeoxidation in the same electrolyte. Bauxite residue is a waste product from the Bayer process to produce aluminium oxide. The high content of iron oxide makes it a candidate for electrodeoxidation in a similar way.

Introduction

Iron and steel production accounts for a considerable amount of total world's anthropogenic CO_2 emissions (1). During recent decades different scenarios and low-emission pathways have been taken up by steelmaking industries together with universities and research institutes to tackle this problem (2). One of the most promising novel processes to replace the current steel making process is the low temperature electrolysis of iron oxide. This process is currently being developed under H2020-ΣIDERWIN project; a European project led by ArcelorMittal. In this process a suspension of iron oxide in a highly alkaline electrolyte (NaOH 50 wt% aqueous solution) is subjected to electrical energy. Hence, the iron oxide is electrochemically reduced to metallic iron at the cathode, while oxygen evolution occurs at the anode. Therefore, this process is capable of producing pure iron with a very low carbon footprint (3,4).

One of the advantages of this process is the fact that in addition to iron oxide (hematite), it is possible to feed this process with other iron-containing raw materials. One alternative raw material which is being studied to be used in this process, is bauxite residue (also known as red mud); the waste material from the Bayer process for alumina production. Bauxite residue usually contains 30-45 wt% iron in the form of oxides and hydroxides. Besides, on average 1-1.5 tons of bauxite residue is produced per ton of alumina (5). Therefore, it is a considerable resource of iron.

Different aspects of this process have been studied so far. However, there are still unknown issues that must be addressed in order to develop the process at an industrial scale. This paper summarizes some of the recent results obtained under ongoing studies in the SIDERWIN project for the development and optimization of this electrochemical process.

These results include cyclic voltammetry studies using a cavity electrode, galvanostatic electrolysis of Fe_2O_3 and bauxite residue suspensions using different cathode materials, electrolysis of pellets and analysis of final products.

Experimental and Materials

The electrolysis experiments were carried out in a polytetrafluoroethylene (PTFE) container (Ø 100 mm, 160 mm height). Different types of working electrodes were used in this study. A rotating disc electrode (RDE) was used for galvanostatic electrolysis tests when the electrolyte was a suspension of Fe_2O_3 or bauxite residue in the NaOH 50 wt% aqueous solution. The RDE body was a PTFE capsule Ø 30 mm, 50 mm long. Three different cathode materials in the form of a rod, Ø 8 mm, was embedded in the PTFE capsule. Two grades of graphite G347 (grade 1) and G348 (grade 2) supplied by Tokai Carbon and a pure silver rod, 99.9 % Alfa Aesar, were used as cathode materials. The properties of these materials are presented in Table I. The PTFE capsule was mounted to the shaft of a modulated speed rotator through the threads made in the capsule and the cathode material; the schematic picture of the RDE is depicted in Figure 1. For cyclic voltammetry studies a cavity electrode was used. This electrode was fabricated similar to the electrodes known as "cavity microelectrodes" in electrochemistry literature. Such electrodes are used for electrochemical studies of materials insoluble in the electrolyte (6). The cavity electrode was made of a PTFE rod, Ø 10 mm and 40 mm long, where a hole of Ø 0.7 mm was drilled into it. A steel rod Ø 4 mm was inserted from the top into the PTFE rod. The steel rod served as current collector; see Figure 1. The powder was crushed in a mortar with pestle and the cavity electrode was pushed on the powder and the cavity was filled with powder. The powder might be consumed after each scan. Between each sweep the cavity electrode was removed from the electrochemical cell, cleaned and reloaded with new powder.

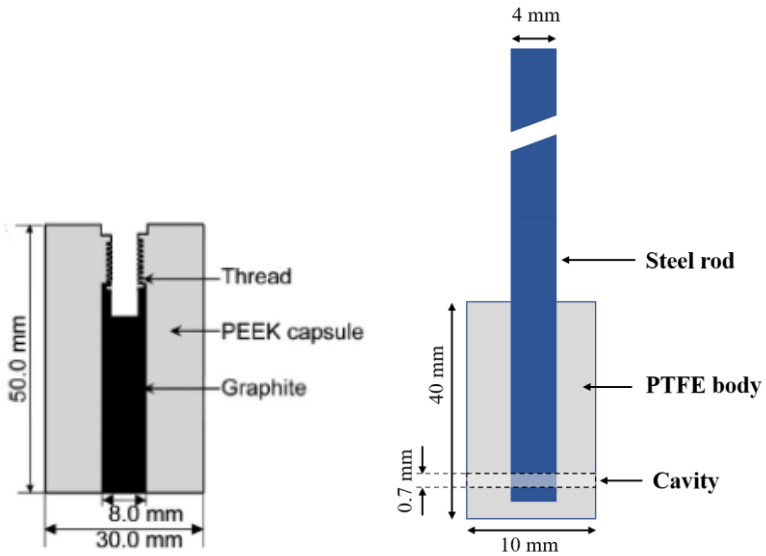

Figure 1. The schematic of rotating disc electrode (left), and cavity electrode (right)

The reference electrode was a commercial single junction Hg/HgO electrode with 4.24 M KOH filling solution (PINE research). It was immersed in a distinct glass compartment

containing 4.2 M KOH solution. This compartment was ionically connected to the electrolyte in the cell with a polyether ether ketone (PEEK) capillary (OD = 1/8", ID = 0.080", Teknolab), whose tip was as close as possible to the working electrode. A silver wire was passed through the PEEK capillary to facilitate the release of gas bubbles. This reference electrode was fabricated according to and similar to the one reported in another study (7). A nickel mesh (Goodfellow, NI008751) was cut in the form of a cylinder (7 mm height and 9 mm diameter). This served as the counter electrode in all experiments. The two sides were fixed together by a Ni wire which also served as the current collector.

Table I. The properties of cathode materials.

	Graphite grade 1	**Graphite grade 2**	**Silver**
Specific gravity (g/cm^3)	1.85	1.92	10.2
Grain size (μm)	11	8	-
Porosity (%)	12	8	None
Specific resistance (μΩm)	11.0	10.0	0.0016
CTE* ($\times 10^{-6}$/°C)	5.5	5.5	19.7

*Coefficient of Thermal Expansion

The electrolyte was a 50 wt% NaOH aqueous solution. Sodium hydroxide (NaOH, Merck 99.0 % pellets) was added and dissolved gradually in Milli-Q water. Then, Iron (III) oxide (Fe_2O_3, Alfa Aesar GmbH & Co KG, 99 %, mesh -325) or bauxite residue powder was added to the NaOH-aqueous solution. The bauxite residue was provided by MYTILINEOS-Aluminium of Greece. The chemical composition is presented in Table II. The mineralogical composition was also provided by X-ray diffraction; see Table III. These data were provided by another group that is using the same bauxite residue.

The PTFE electrolysis cell had a lid. This lid was used to feed through the PTFE mechanical stirrer, the working electrode, the lead to the nickel mesh (counter electrode), a thermometer, and the capillary PEEK connected to the reference electrode in the cell. The cell was placed inside a beaker containing a silicone oil supplied by Alfa Aesar. The beaker itself was placed on a magnetic stirring hotplate. The beaker served as heating bath for the electrolysis cell.

TABLE II. Chemical composition of bauxite residue (8)

No.	**Species**	**Weight percentage**
1	Fe_2O_3	44.8
2	Al_2O_3	18.6
3	SiO_2	6.7
4	CaO	9.8
5	Na_2O	2.9
6	TiO_2	6.7
7	LIO	9.2
	Total	98.5

Table III. Mineralogical analysis of bauxite residue (8)

No.	Mineral name
1	Hematite
2	Hydrogarnet
3	Diaspore
4	Cancrinite
5	Goethite
6	Calcite
7	Perovskite
8	Chamosite
9	Gibbsite
10	Boehmite
11	Portlandite
12	Rutile
13	Anatase
14	Quartz

In addition, some electrolysis tests were carried out using a pellet made of hematite/bauxite residue. In such studies a pellet or tablet of the raw material is prepared and attached to the cathodic current collector. This is in a way similar to the well-known FCC Cambridge process which was developed for electrochemical reduction of titanium oxides in molten salts (9). For this purpose, pellets of iron oxide and bauxite residue were prepared by pressing the powder in a uniaxial press with a force of 3 N for 1 min. The pressing was performed using a specially fabricated die with a thin gap along its wall which allowed passing a Pt wire through it. This Pt wire, Ø 6 mm and 20 mm long, served as the cathode current collector. The pressing procedure was followed by sintering the iron oxide and bauxite residue pellets in air, for 3-4 h and at 800 °C and 1100 °C, respectively. In case of bauxite residue pellets, a calcination procedure (in air, at 600 °C, 6 h long) was done prior to pressing and making the pellets. This procedure was necessary to ensure the mechanical stability of the pellets by removing some of the hydrates present in bauxite residue.

All the electrochemical measurements were carried out using a PARSTAT 4000A, AMETEK Scientific Instruments electrochemical workstation. The samples were analyzed by X-ray diffraction (XRD) Bruker D8 A25 DaVinci X-ray Diffractometer with Cu-Kα radiation and Scanning Electron Microscope (SEM) Hitachi S-3400N equipped with Energy Dispersive X-Ray Spectroscopy (EDS).

Results and discussion

Cyclic voltammetry

As stated earlier, voltammetry studies were carried out using a cavity electrode. Figure 2 shows the voltammogram using a cavity electrode filled with Fe_2O_3 particles, with scan rate equal to 20 mV/s. The cathodic current started gradually from ~-0.6 V (versus reference electrode). This cathodic current cannot be due to hydrogen evolution since it occurs at a more negative potential. Hence, this cathodic current must be the result of reduction of Fe_2O_3. As the potential moved to more negative values it merged with hydrogen evolution. Considering previous studies, this cathodic reaction can be attributed

to direct electrochemical reduction of the Fe_2O_3 to o Fe (0). This suggests that the reduction of Fe_2O_3 to metallic iron occurred in one step. This result is expected and agrees with previous studies (10-13); as Fe_2O_3 particles were present and attached to the current collector in the cavity electrode arrangement. The anodic peak corresponding to metallic iron dissolution can also be clearly seen. Besides, the second and third scans were almost the same as the first one.

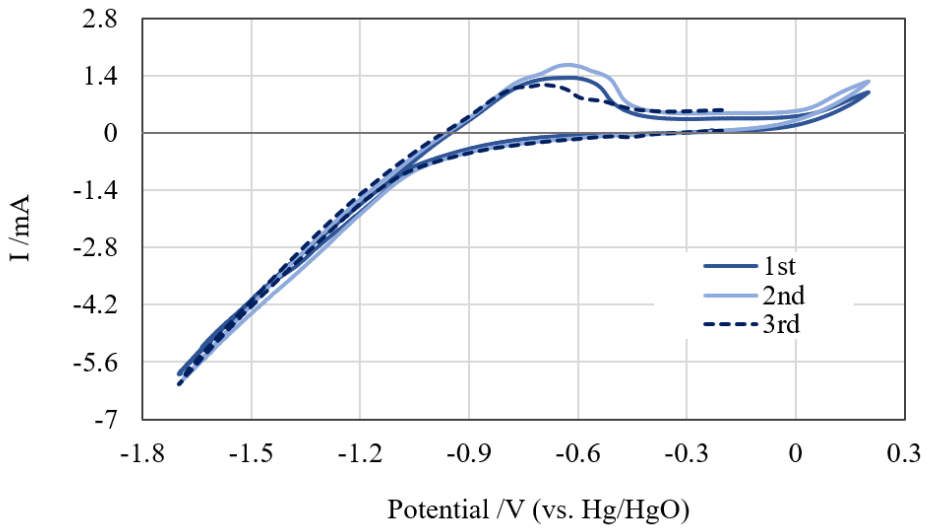

Figure 2. Cyclic voltammogram of Fe_2O_3 particles in a cavity electrode, scan rate: 20 mV/s.

The voltammogram from bauxite residue sample is given in Figure 3. Like the voltammogram from Fe_2O_3 sample, here again the cathodic current started from ~-0.6 V (vs. RE) and at more negative potentials merged to hydrogen evolution. However, it seemed there was another cathodic reaction involved. There was a second peak at ~-1.0 V which can only be observed in the first scan; (see the embedded picture in Figure 3). Besides, on the reverse scan there were obviously two anodic peaks. This suggests that there was probably another cathodic reaction involved. One possibility is that this is due to electrochemical reduction of SiO_2. The fact that the bauxite residue powder is a mixture of different oxides can explain why this second cathodic peak did not appear in the second and third scans. Another possibility is that hematite reduced in two steps: reduction of Fe III to Fe II and Fe II to Fe (0); as it was reported in one study where a suspension of bauxite residue in the same electrolyte, was studied. However, in that study the two cathodic peaks were detected at different potentials (8). Nevertheless, the fact that in that study a suspension of bauxite residue was studied and here it was bauxite residue powder inside the cavity electrode can be the reason for these differences.

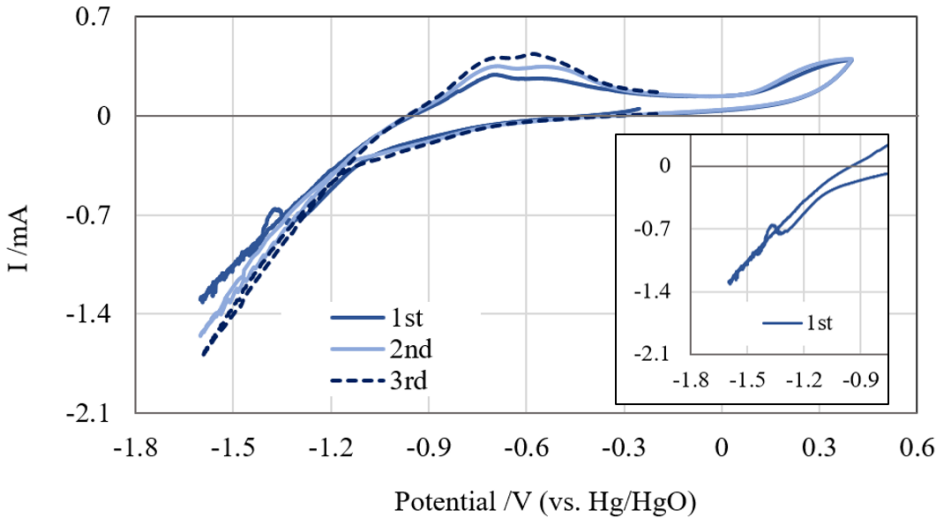

Figure 3. Cyclic voltammogram of bauxite residue, scan rate: 20 mV/s, cavity electrode

Galvanostatic electrolysis of suspension

As stated earlier, rotating disc electrodes with three different cathode materials were used for galvanostatic electrolysis tests. All the electrowinning testes were carried out at constant current with current density equal to 0.2 Acm^{-2}. During electrowinning the suspension was stirred with mechanical stirrer at 60-100 rpm and the temperature was ~100 °C. Table IV summarizes the results from these tests. The apparent current efficiency (presented as A. CE in Table IV) was calculated based on weight gain of the cathode after electrolysis. As can be seen, in the experiments where Fe_2O_3 was the iron-containing raw material the highest current efficiency was achieved by using silver cathode. The graphite grade 2, which had less porosity compared to grade 1, performed better and higher current efficiency was achieved. It must be noted that in these experiments the RDE was not rotating. If these results are compared with the results from a similar study with a similar setup (4), it becomes clear that the obtained current efficiencies were rather high; considering the fact that the RDE was not rotating. This was probably due to the fact that the graphite grades used here were dense with low porosity. This enhanced the bonding of deposited iron to the cathode surface. Obviously, silver had no porosity and gave the best results.

The variation of cathode potentials with time for sample 2 is depicted in Figure 4. The other samples showed similar variations for cathode potentials and cell voltage. At the beginning the cathode potential was high and as time passed the cathode potential decreased and after 20-30 min it became stable. This was because after the first layers of iron deposited on the cathode then the deposition of successive layers of iron became easier and less energy is required for deposition of iron on previously deposited iron. The cell voltage was measured during electrolysis. The cell voltage variation followed the changes of cathode potential. It seems that the anode potential did not change much during electrolysis and probably only at the very beginning.

Table IV. Results of galvanostatic electrolysis tests using suspensions of hematite and bauxite residue. Here, G, A. CE, IO and BR respectively stand for grade (graphite), apparent current efficiency, iron oxide and bauxite residue.

Sample. No.	Cathode	A. CE /%	Raw material	Conc. /wt. %	RDE /rpm
1	G1	72	IO	26	Non rot.
2	G2	86	IO	26	Non rot.
3	Ag	95	IO	26	Non rot.
4	G1	36	BR	S/L: 100	1000 rpm
5	Ag	34	BR	S/L: 100	1000 rpm
6	G1	41	BR	S/L: 200	1000 rpm
7	G2	39	BR	S/L: 200	1000 rpm

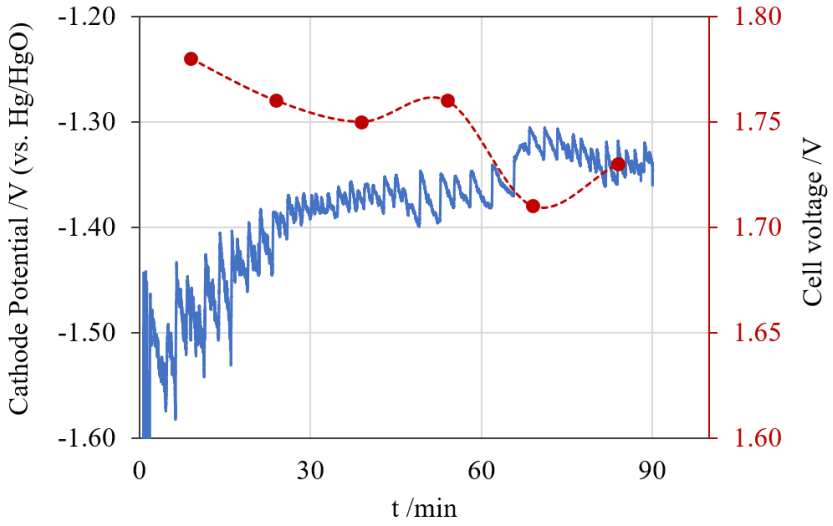

Figure 4. The variations of cathode potential and cell voltage with time during galvanostatic electrolysis of Fe_2O_3 suspension in the electrolyte. Cathode material was graphite grade 1.

In electrolysis of bauxite residue suspension, the concentration of bauxite residue was defined by the ratio of solid (bauxite residue) to liquid (NaOH aqueous solution). In these tests much lower current efficiencies were obtained; see Table IV. This was probably due to the presence of nonreactive particles which can cover the cathode surface and hinder the reduction of electrochemically active particles (such as Fe_2O_3). Nevertheless, there might be other reasons which affected the electrochemical reduction and led to lower current efficiencies compared to pure Fe_2O_3. In another study with a similar setup and under similar conditions almost the same values of current efficiency were reported. Furthermore, by increasing the temperature (up to 130 °C), much higher current efficiency (~70%) was achieved (8). As expected, when the concentration of bauxite residue in the electrolyte was higher the current efficiency increased. Figure 5 illustrates the variation of cathode potential and cell voltage versus time during two electrolysis tests of bauxite residue; Figure 5-top illustrates these changes for the sample with silver cathode and solid/liquid ratio equal to 100 g/l and Figure 5-below depicts the curves of the sample with graphite cathode (grade 2) and solid/liquid ratio equal to 200 g/l. Here again the curves depicting the variations of cathode potential and the cell voltage were similar to those obtained during electrolysis of Fe_2O_3 (see Figure 4 and notice that the electrolysis duration for Fe_2O_3 was 30 minutes shorter). Higher concentration of bauxite residue did not change the values of

cathode potential and cell voltage. In fact, the lower value of the cathode potential in Figure 5-top is due to the silver cathode material; similar to what was observed during electrolysis of Fe_2O_3 suspension. On average, for the samples where the cathode material was graphite (not all presented here) the cathode potential started from -1.6 V and after about 30 min reached stable value of -1.3 V. The cell voltage value was almost the same and with similar changes for all samples.

Repeated use of the same electrolyte resulted in lower current efficiencies. This could be due to accumulation of oxygen in the electrolyte and/or settling of the bauxite residue in the cell. The latter was also reported in another study as change in homogeneity of the suspension (4). Even adding more bauxite residue to this electrolyte led to lower current efficiencies. This is probably due to the fact that the viscosity of the solution increased and adversely affected the mass transfer.

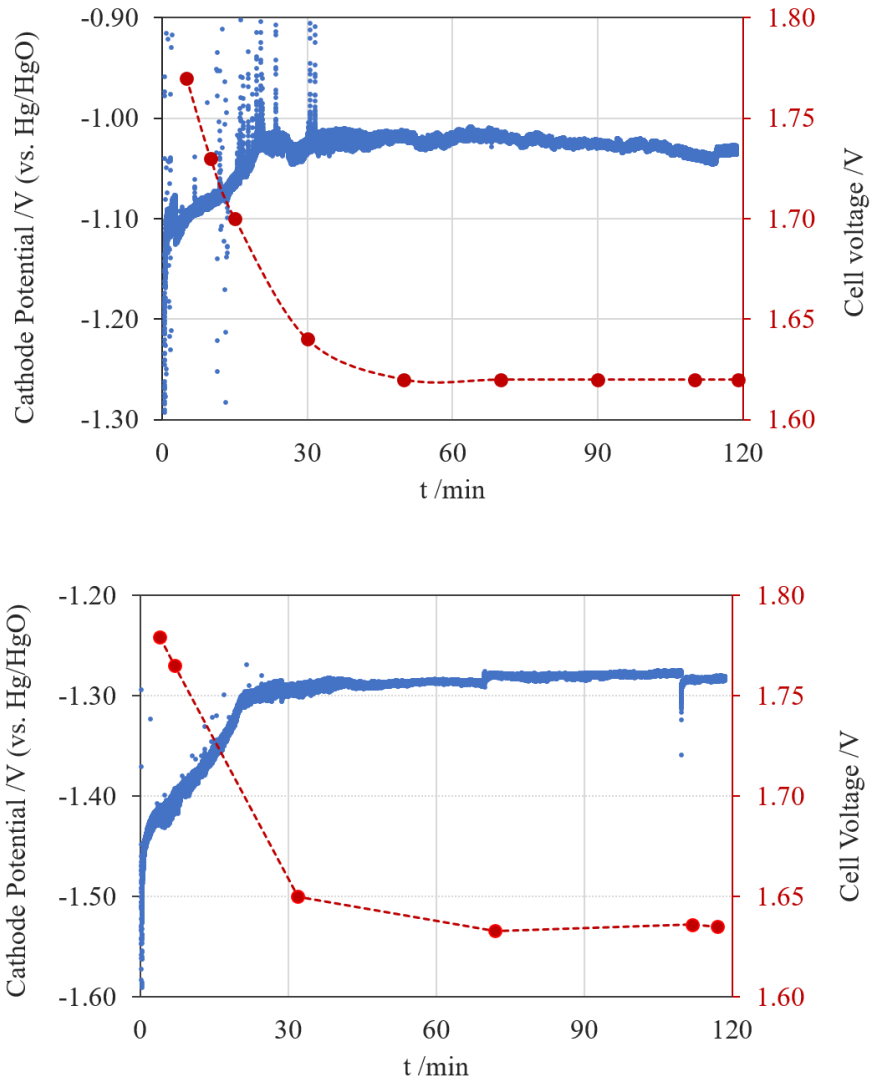

Figure 5. The variations of cathode potential and cell voltage with time during galvanostatic electrolysis of bauxite residue suspension in the electrolyte. Cathode: silver, S/L = 100 g/l (top) and Cathode: graphite grade 2, S/L = 200 g/l (below).

Microscopy studies

Figure 6 shows the SEM images of deposits obtained after electrowinning of Fe_2O_3 and bauxite residue containing suspensions. Figure 6 (a) to (c) are images of iron deposits obtained after electrowinning of Fe_2O_3. The microstructure of deposited iron was similar to those obtained in previous studies (4,12). The iron crystals were made up of six twin crystals; the twin crystals were tetrahedron-shaped and converged at an apex (Figure 6-a). However, the deposit was not very compact which is due to the fact that the RDE was not rotating (Figure 6-b and c); as reported in another study (4).

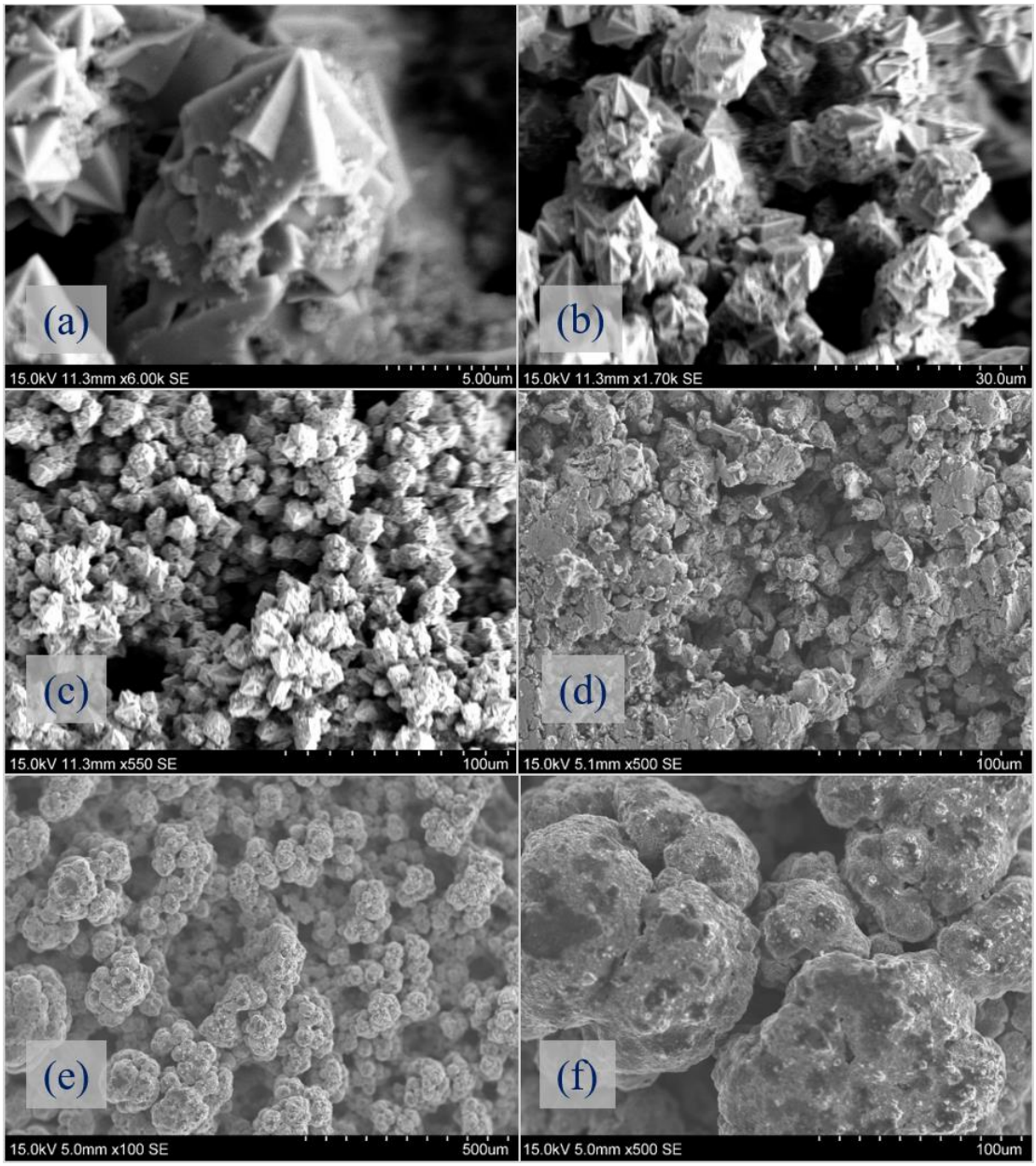

Figure 6. SEM images of deposits from electrowinning of Fe2O3 and bauxite residue.

Figure 6 (d) to (f) are from bauxite residue samples. Here the iron deposit has a different microstructure. The tetrahedron-shaped twin crystals could not be observed (However images with higher magnification could probably reveal the crystals). The presence of

different impurities affected the microstructure of deposited iron. This was also reported in a former study where electrowinning was performed using a mixture of Fe_2O_3, SiO_2 and Al_2O_3 (14). In bauxite residue there were other impurities as well. Besides, the hematite in bauxite residue is different from pure Fe_2O_3.

Galvanostatic electrolysis of pellets

In addition to electrowinning tests, another approach was also taken in this study. Pellets made of Fe_2O_3 and bauxite residue particles were prepared as explained before. These were applied to constant current electrolysis. The operating conditions were the same as for electrowinning tests except that the electrolyte was not stirred. Table V summarizes the results of these tests. The apparent current efficiency for each electrolysis test was calculated based on the weight change of the pellets during electrolysis.

Table V. Galvanostatic electrolysis of pellets. Here, A. CE, IO and BR respectively stand for apparent current efficiency, iron oxide and bauxite residue.

Sample No.	t /min	Raw material	A. CE /%
1	100	IO	34
2	200	IO	46
3	200	BR	3
4	400	BR	13
5	700	BR	11

X-ray diffraction analysis of the pellets after electrolysis revealed the final phases. After 200 min, which was the theoretical required time for complete reduction of Fe_2O_3 pellet, this sample consisted of a mixture of metallic iron and remaining Fe_2O_3. An earlier study had shown that complete reduction of Fe_2O_3 pellet can be achieved after much longer electrolysis; ~19 h (15). Regarding the bauxite residue pellets these tests showed that 700 min electrolysis was not enough to convert all the hematite to metallic iron. However, all the hematite in the pellet had reduced either to metallic iron or magnetite: no hematite could be detected after 700 min electrolysis. XRD also revealed that the other comprising phases in the bauxite residue pellet were $CaTiO_3$ (perovskite) and Al_2O_3 (corundum). Of course, there were probably other phases present in the sample, but their percentage was lower than the detection limit of XRD. These results suggest that as a result of electrolysis, Fe_2O_3 is directly converted to metallic iron. However, the electrochemical reduction of hematite present in the bauxite residue occurs through conversion of hematite to magnetite, and then magnetite to metallic iron.

Conclusions

The electrochemical reduction of Fe_2O_3 and bauxite residue in NaOH-H_2O (50-50 wt%) electrolyte was studied. A cavity electrode was used to run cyclic voltammetry tests and electrochemical redox reactions were successfully observed and studied. It seems minor changes in the cavity electrode, such as a shorter cavity length, might improve the precision and accuracy of the voltammograms. Among different materials tested as cathode, silver showed a better performance. It was also demonstrated that in addition to Fe_2O_3, bauxite residue can as well be used as a raw material in this process and iron can successfully be recovered. Though, the process must be optimized to achieve higher efficiencies.

Acknowledgments

The financial support provided from the European Union H2020 SIDERWIN project is greatly appreciated.

References

1. Worldsteel.org
2. M. Abdul Quader, S. Ahmed, S.Z. Dawal, and Y. Nukman, *Renew. Sust. Energ. Rev.*, **55**, (2016).
3. A. Allanore, H. Lavelaine, G. Valentin, J.P. Birat, and F. Lapicque, *J. Electrochem. Soc.*, **154** (12), (2007).
4. B. Yuan, O.E. Kongstein, and G.M. Haarberg, *J. Electrochem. Soc.*, **156** (2), (2009).
5. K. Tsesmelis, Bauxite Mine Rehabiliation & Bauxite Residue Management: A Global Perspective, in Proc. 35th Int. ICSOBA Conf., ICSOBA, (2017).
6. G. Qiu, M. Ma, D. Wang, X. Jin, X. Hu, and G.Z. Chen, *J. Electrochem. Soc.*, **152** (10), (2005).
7. V. Feynerol, H. Lavelaine, P. Marlier, M.-N. Pons, and F. Lapicque, *J. App. Electrochem.*, **47**, (2017).
8. S. Koutsoupa1, S. Koutalidi, E. Bourbos, E. Balomenos, and D. Panias, Submitted to *JOHNSON MATTHEY TECH*.
9. G.Z. Chen, D.J. Fray, and T.W. Farthing, *Nature.*, **407**, (2000).
10. A. Allanore, H. Lavelaine, G. Valentin, J.P. Birat, P. Delcroix, and F. Lapicque, *Electrochim. Acta.*, **55**, (2010).
11. A. Allanore, H. Lavelaine, G. Valentin, J.P. Birat, and F. Lapicque, *J. Electrochem. Soc.*, **155**, (2008).
12. M. Tokushige, O.E. Kongstein, and G.M. Haarberg, *ECS Trans.*, **50** (52), (2013).
13. M. Siebentritt, P. Volovtich, K. Ogle, and G. Lefevre, *Colloids Surf. A Physicochem. Eng. Asp.*, 440, (2014).
14. S.H. Tang and G.M. Haarberg, *ECS Trans.*, **28** (6), (2010).
15. G.M. Haarberg and B. Yuan, *ECS Trans.*, **58** (20), (2013).